A novel 2.5D method for solving the mixed boundary value problem of a surface effect ship

Zhiqun Guo[1], Q.W. Ma[2,1,*], Hongde Qin[1]

[1] College of Shipbuilding Engineering, Harbin Engineering University

[2] School of Engineering and Mathematical Sciences, City University London

* Correspondence: Q.Ma@city.ac.uk

Abstract: When a surface effect ship (SES) sails in waves, the unsteady velocity potential of water can be decomposed into incident potential, sidehull radiation potential, sidehull diffraction potential and radiation potential due to fluctuating air pressure. The potentials related to sidehulls satisfy Neumann boundary conditions (BC) and have been successfully addressed using the 2.5D method. In contrast, the potential related to fluctuating air pressure satisfies mixed BC consisting of homogeneous Neumann BC on the wetted surface of sidehulls and nonhomogeneous Dirichlet BC on the interface between air and water, which has never been studied using the efficient 2.5D method. In this paper, the 2.5D method is firstly proposed to solve the mixed boundary value problem (BVP), which can deal with the coupling between the fluctuating air pressure and sidehulls. By using the 2.5D method, the radiation wave and other relative hydrodynamic parameters of a SES due to the fluctuating air pressure are evaluated. The numerical results on motion response and the fluctuated air pressure of the SES show acceptable agreement with the experimental ones.

Keywords: 2.5D method; mixed boundary value problem; surface effect ship; air cushion

---

1. Introduction

The surface effect ship (SES) is a kind of high speed vessel widely used in the marine transportation. When navigating in waves, the SES makes unsteady motions, and the pressure in the air cushion fluctuating due to the pumping effect of waves. Inversely, the unsteady motions of sidehulls and the fluctuating air pressure can have influence on the motion of water, which induce the sidehull radiation potential, sidehull diffraction potential and radiation potential due to fluctuating air pressure. One needs to solve all of these velocity potentials for reckoning the responses of the SES in waves.

The sidehull radiation and diffraction potentials satisfy nonhomogeneous Neumann boundary condition (BC) on the wetted surface of sidehulls and homogeneous Dirichlet BC on the interface between air cushion and water. The latter is actually similar to the conventional free surface condition, which makes the sidehull radiation and diffraction potentials obtained by simply solving Neumann boundary value problems (BVP). In this sense, the hydrodynamics of the SES sidehulls is the same as conventional catamarans. 3D numerical methods such as Rankine source method (Connell *et al*., 2011), finite element method (García-Espinosa *et al*., 2015) and URANS method (Bhushan *et al*., 2017) have been employed in literature to precisely evaluate the hydrodynamics of SES sidehulls. However, the 3D methods are computationally expensive and might not meet the engineering demands. For example, it is not suitable for establishing an SES motion control model by incorporating the 3D methods into the control models (Karimi *et al*., 2005a; Karimi *et al*., 2010; Zhang *et al*., 2015) due to its low computational

efficiency of the methods. To enhance the computational efficiency, Guo *et al*. (2015) employed the 2.5D method to calculate the hydrodynamic coefficients of a special SES, which is called Partial Air Cushion Supported Catamaran (PACSCAT). The 2.5D method is very efficient because the free surface condition in it is kept three-dimensional, while the governing equations and body surface conditions are reduced to two-dimensional (Faltinsen and Zhao, 1991; Ma *et al*., 2005).

On the other hand, the radiation potential due to fluctuating air pressure satisfies the mixed BC consisting of homogeneous Neumann BC and nonhomogeneous Dirichlet BC, the latter of which is built through the Bernoulli's equation. To obtain the radiation potential due to fluctuating air pressure, one has to solve the mixed BVP. The 3D numerical methods can be utilized to do so, but they still consume a significant amount of computational resources. For the sake of simplicity, in some works (Doctors, 1976; Xie *et al*., 2008) the mixed BVP was simplified to a Dirichlet BVP, i.e. the homogeneous Neumann BC as well as the coupling between the fluctuating air pressure and sidehulls was neglected. The simplification, however, inevitably has impact on the numerical precision and thus one cannot obtain the accurate radiation potential due to fluctuating air pressure.

A possible approach to overcome the aforementioned difficulties is to exploit the 2.5D method to solve the mixed BVP, which has advantages of accuracy and efficiency. However, the 2.5D method generally was exploited to solve the Neumann BVP (Faltinsen and Zhao, 1991; Ma *et al*., 2005; Guo *et al*., 2015), i.e. hydrodynamic problems of displacement or planing ships, or the Dirichlet BVP (Guo *et al*., 2017), i.e. hydrodynamic problems of hovercrafts, and has never been employed to solve the mixed BVP.

In this paper, the 2.5D method is firstly employed to solve the mixed BVP arising from the unsteady motions of a SES. By using the 2.5D method, we solve the radiation potential due to fluctuating air pressure, as well as the radiation waves on the interface and radiation forces on the wetted surface of sidehulls. The obtained results are substituted into the motion equations of a PACSCAT to find the motion response and the fluctuating air pressure in the air cushion. The numerical results are compared with the experimental data in a few cases. The object of the present paper is to provide an efficient and accurate method to evaluate the hydrodynamics of air cushion in a SES.

2. Mathematical model of the mixed BVP and corresponding 2.5D numerical method

Let $O-XYZ$ be an earth-fixed coordinate system and $o-xyz$ a SES-accompanied coordinate system. The latter is always parallel to $O-XYZ$. When the SES is at its mean position, the x-axis is pointing upstream parallel to the longitudinal plane of the SES and the z-axis is pointing vertically upward through the center of gravity (COG) of the SES. The origins of both coordinate systems are located in the plane of mean free surface.

2.1. Governing equations for hydrodynamics of the SES

Let $\Phi_{\mathrm{I}}=\eta_0\phi_{\mathrm{I}}\mathrm{e}^{\mathrm{i}\omega t}$ be the incident wave, where η_0 is the wave amplitude, ϕ_{I} the spatial component of Φ_{I} with an unit amplitude, ω the encountered frequency. Within the framework of linear assumption, the unsteady disturbed velocity potential around the SES can be written as

$$\phi_{\mathrm{T}}=\phi_{\mathrm{D}}+\phi_{\mathrm{R}}+\phi_{\mathrm{P}}=\left\{\eta_0\phi_0+\sum_{j=1}^{6}\eta_j\phi_j+\sum_{j=7}^{6+N_{\mathrm{P}}}\eta_j\phi_j\right\}\mathrm{e}^{\mathrm{i}\omega t} \tag{1}$$

where $\phi_{\mathrm{D}},\phi_{\mathrm{R}},\ \phi_{\mathrm{P}}$ are sidehull diffraction potential, sidehull radiation potential and radiation potential due to fluctuating air pressure, respectively; ϕ_0 the spatial component of ϕ_{D} corresponding due the unit amplitude of

the incident wave, $\phi_j(j=1,\dots,6)$ the spatial component of ϕ_{R} in j-th motion mode of an unit amplitude, $\phi_j(j=7,\dots,6+N_{\mathrm{P}})$ the spatial component of ϕ_{P} in j-th mode, $\eta_j\ (j=1,\dots,6)$ the amplitude of j-th motion mode, $\eta_j(j=7,\dots,6+N_{\mathrm{P}})$ the equivalent waterhead of the fluctuating air pressure in j-th mode, N_{P} the number of modes.

The fluctuating air cushion pressure on the interface can be expressed as

$$\tilde{p}(x,y,t)=\hat{p}(x,y)\mathrm{e}^{\mathrm{i}\omega t}=-\rho_{\mathrm{w}}\mathrm{g}\mathrm{e}^{\mathrm{i}\omega t}\sum_{j=7}^{6+N_{\mathrm{P}}}\eta_j N_j(x,y) \tag{2}$$

where $\hat{p}(x,y)$ is the spatial component of $\tilde{p}(x,y,t)$, ρ_{w} the density of water, g the gravity, $N_j(x,y)$ a complete set of orthogonal Fourier modes expanded on the interface defined as (Lee and Newman, 2015)

$$N_j(x,y)=\begin{pmatrix}\cos(\alpha\pi(x-x_{\mathrm{m}})/l)\\ \sin(\alpha\pi(x-x_{\mathrm{m}})/l)\end{pmatrix}\begin{pmatrix}\cos(\beta\pi y/b)\\ \sin(\beta\pi y/b)\end{pmatrix} \tag{3}$$

where α,β are even for the modes corresponding to the cosine or odd for the sine; l,b,x_{m} are the length, breadth, and longitudinal center of the air cushion, respectively.

According to the Bernoulli's equation, the boundary condition on the interface between water and air is

$$\sum_{j=7}^{6+N_{\mathrm{P}}}\eta_j\left(\left(\mathrm{i}\omega-U\frac{\partial}{\partial x}\right)^2+\mathrm{g}\frac{\partial}{\partial z}\right)\phi_j=\mathrm{g}\sum_{j=7}^{6+N_{\mathrm{P}}}\eta_j\left(\mathrm{i}\omega-U\frac{\partial}{\partial x}\right)N_j(x,y) \tag{4}$$

where U is the forward speed of the SES.

If the sidehulls of the SES are slender and the forward speed is high (the Brard number $U\omega/\mathrm{g}$ is far larger than 0.25 (Ma *et al*., 2005)), the high-speed slender body assumption could be applied to the sidehulls of the SES, under which the surge potential ϕ_1 is neglected. Then the BVP for the sidehull radiation and diffraction potentials $(\phi_j, j=0,2,\dots,6)$ can be formulated as

$$\begin{cases}\dfrac{\partial^2\phi_j}{\partial y^2}+\dfrac{\partial^2\phi_j}{\partial z^2}=0, & \text{in } \Omega\\ \left[\left(\mathrm{i}\omega-U\dfrac{\partial}{\partial x}\right)^2+\mathrm{g}\dfrac{\partial}{\partial z}\right]\phi_j=0, & \text{on } S_{\mathrm{F}}\cup S_{\mathrm{P}}\\ \dfrac{\partial\phi_j}{\partial n}=\begin{cases}\mathrm{i}\omega n_j+Um_j, & j=2,\dots,6\\ -\dfrac{\partial\phi_{\mathrm{I}}}{\partial n}, & j=0\end{cases}, & \text{on } S_{\mathrm{B}}\\ \phi_j=\dfrac{\partial\phi_j}{\partial x}=0, & \text{at } x>x_0\\ \phi_j=\nabla\phi_j=0, & \text{on } S_\infty\end{cases} \tag{5}$$

where $\Omega, S_{\mathrm{B}}, S_{\mathrm{P}}, S_{\mathrm{F}}, S_\infty$ are the fluid domain enclosed by the mean wetted body surface S_{B}, the mean interface S_{P} between air cushion and water, the mean free surface S_{F}, the boundary S_∞ at infinity; x_0 is the x-coordinate of the bow; $n_j(j=1,\dots,6)$ is the generalized normal vector, and m_j is defined as $(m_1,m_2,m_3)=(0,0,0)$ and $(m_4,m_5,m_6)=(0,n_3,-n_2)$.

Analogously, if the air cushion is slender (the ratio of the length to beam l/b is larger than 2 (Guo *et al*., 2017)) and the forward speed is high (the Froude number F_{rl} is larger than 0.4 (Guo *et al*., 2017)), the high-speed slender body assumption could also be applied to the air cushion of the SES. Then the BVP for radiation potentials due to fluctuating air pressure $(\phi_j, j=7,\dots,6+N_{\mathrm{P}})$ can be formulated as

$$\begin{cases} \frac{\partial^2\phi_j}{\partial y^2}+\frac{\partial^2\phi_j}{\partial z^2}=0, & \text{in } \Omega \\ \left(\left(\mathrm{i}\omega-U\frac{\partial}{\partial x}\right)^2+\mathrm{g}\frac{\partial}{\partial z}\right)\phi_j=\begin{cases}\mathrm{g}\left(\mathrm{i}\omega-U\frac{\partial}{\partial x}\right)N_j(x,y), \\ 0,\end{cases} & \begin{matrix}\text{on } S_\mathrm{P} \\ \text{on } S_\mathrm{F}\end{matrix} \\ \frac{\partial\phi_j}{\partial n}=0, & \text{on } S_\mathrm{B} \\ \phi_j=\frac{\partial\phi_j}{\partial x}=0, & \text{at } x>x_0 \\ \phi_j=\nabla\phi_j=0, & \text{on } S_\infty \end{cases} \tag{6}$$

The mixed BVP (6) is a novel model presented in this work, in which the sidehull effects on the velocity potential due to pressure are firstly considered. In contrast, in previous papers (Xie *et al*., 2008; Guo *et al*., 2015) the sidehull effects were ignored. Obviously, Eq.(5) and Eq.(6) are Neumann BVP and mixed BVP, respectively. The Neumann BVP (5) has be successfully solved using the 2.5D method (Ma *et al*., 2005), while the mixed BVP (6) has never been tried using the 2.5D method.

2.2. The mixed BVP solved using the 2.5D method

The 2.5D method resolves a 3D frequency-domain BVP by converting it into one defined in a 2D time-domain. To do so, the following variable substitutions need to be made

$$\begin{cases} x(t)=x_0-Ut \\ \psi_j(t,y,z)=\mathrm{e}^{\mathrm{i}\omega t}\phi_j(x(t),y,z) \\ \Pi_j(t,y)=\mathrm{e}^{\mathrm{i}\omega t}N_j(x(t),y) \end{cases} \tag{7}$$

Substituting Eq.(7) into the 3D frequency-domain BVP (6) yields a 2D time-domain BVP

$$\begin{cases} \frac{\partial^2\psi_j}{\partial y^2}+\frac{\partial^2\psi_j}{\partial z^2}=0, & \text{in } \Omega \\ \frac{\partial^2\psi_j}{\partial t^2}+\mathrm{g}\frac{\partial\psi_j}{\partial z}=\begin{cases}\mathrm{g}\frac{\partial\Pi_j}{\partial t}, \\ 0,\end{cases} & \begin{matrix}\text{on } S_\mathrm{P} \\ \text{on } S_\mathrm{F}\end{matrix} \\ \frac{\partial\psi_j}{\partial n}=0, & \text{on } S_\mathrm{B} \\ \psi_j=0, & t\le 0 \\ \frac{\partial\psi_j}{\partial t}=\begin{cases}\mathrm{g}\Pi_j(0,y), \\ 0,\end{cases} & \begin{matrix}t=0,\ \text{on } S_\mathrm{P} \\ t=0,\ \text{on } S_\mathrm{F}\end{matrix} \\ \psi_j=\nabla\psi_j=0, & \text{on } S_\infty \end{cases} \tag{8}$$

The 2D time-domain free surface Green's function is proposed to solve the time-domain mixed BVP (8):

$$G(\boldsymbol{p},t;\boldsymbol{q},\tau)=\delta(t-\tau)\ln\frac{r_{pq}}{r_{p\bar{q}}}-H(t-\tau)\tilde{G}(\boldsymbol{p},t;\boldsymbol{q},\tau) \tag{9}$$

$$\tilde{G}(\boldsymbol{p},t;\boldsymbol{q},\tau)=2\int_0^\infty\sqrt{\mathrm{g}/k}\,\mathrm{e}^{k(z+\zeta)}\cos(k(y-\eta))\sin\left(\sqrt{\mathrm{g}k}(t-\tau)\right)\mathrm{d}k \tag{10}$$

where $\boldsymbol{p},\boldsymbol{q}$ and $\bar{\boldsymbol{q}}$ are the field point, source point and the mirror of source point about the mean free surface, respectively; r_{pq} and $r_{p\bar{q}}$ are the distance from $\boldsymbol{p}$ to $\boldsymbol{q}$ and from $\boldsymbol{p}$ to $\bar{\boldsymbol{q}}$, respectively; $\delta(\cdot)$ and $H(\cdot)$ are Dirac and Heaviside functions, respectively; $\tilde{G}$ is the free surface memory term of the Green's function.

Applying the Green's theorem to $\psi_j(\tau,\boldsymbol{q})$ and $\tilde{G}(\boldsymbol{p},t;\boldsymbol{q},\tau)$, one gets

$$\int_{S_\mathrm{F}+S_\mathrm{B}+S_\mathrm{P}+S_\infty}\left(\psi_j\frac{\partial\tilde{G}}{\partial n_q}-\tilde{G}\frac{\partial\psi_j}{\partial n_q}\right)\mathrm{d}s_q=0 \tag{11}$$

It is well known that the integral on S_∞ in Eq.(11) is equals to 0. Considering this and integrating Eq.(11) over τ yields

$$\int_0^t \mathrm{d}\tau \int_{S_\mathrm{F}+S_\mathrm{B}+S_\mathrm{P}} \left(\psi_j \frac{\partial \tilde{G}}{\partial n_q} - \tilde{G} \frac{\partial \psi_j}{\partial n_q}\right) \mathrm{d}s_q = 0 \tag{12}$$

Using the free surface condition, the integral on S_P in Eq.(12) comes to

$$\int_0^t \mathrm{d}\tau \int_{S_\mathrm{P}} \left(\psi_j \frac{\partial \tilde{G}}{\partial n_q} - \tilde{G} \frac{\partial \psi_j}{\partial n_q}\right) \mathrm{d}s_q = \int_{S_\mathrm{P}} \psi_j \frac{\partial}{\partial \zeta} \ln \frac{r_{pq}}{r_{p\bar{q}}} \mathrm{d}s_q + \int_0^t \mathrm{d}\tau \int_{S_\mathrm{P}} \Pi_j(\tau, \eta) \frac{\partial \tilde{G}}{\partial \tau} \mathrm{d}s_q \tag{13}$$

Analogously, using the interface condition, the integral on S_F reads

$$\int_0^t \mathrm{d}\tau \int_{S_\mathrm{F}} \left(\psi_j \frac{\partial \tilde{G}}{\partial n_q} - \tilde{G} \frac{\partial \psi_j}{\partial n_q}\right) \mathrm{d}s_q = \int_{S_\mathrm{F}} \psi_j \frac{\partial}{\partial \zeta} \ln \frac{r_{pq}}{r_{p\bar{q}}} \mathrm{d}s_q \tag{14}$$

On the other hand, applying Green's theorem to $\psi_j(\tau, \boldsymbol{q})$ and $\ln \frac{r_{pq}}{r_{p\bar{q}}}$, one obtains

$$\begin{aligned} &2\pi\psi_j(t, \boldsymbol{p}) - \int_{S_\mathrm{B}} \left(\psi_j(t, \boldsymbol{q}) \frac{\partial}{\partial n_q} \ln \frac{r_{pq}}{r_{p\bar{q}}} - \ln \frac{r_{pq}}{r_{p\bar{q}}} \frac{\partial \psi_j(t, \boldsymbol{q})}{\partial n_q}\right) \mathrm{d}s_q \\ &= \int_{S_\mathrm{F}} \psi_j(t, \boldsymbol{q}) \frac{\partial}{\partial \zeta} \ln \frac{r_{pq}}{r_{p\bar{q}}} \mathrm{d}s_q + \int_{S_\mathrm{P}} \psi_j(t, \boldsymbol{q}) \frac{\partial}{\partial \zeta} \ln \frac{r_{pq}}{r_{p\bar{q}}} \mathrm{d}s_q \end{aligned} \tag{15}$$

Combining Eqs.(12)~(15) yields the boundary intergral equation (BIE)

$$\begin{aligned} &2\pi\psi_j(t, \boldsymbol{p}) - \int_{S_\mathrm{B}} \left(\psi_j(t, \boldsymbol{q}) \frac{\partial}{\partial n_q} \ln \frac{r_{pq}}{r_{p\bar{q}}} - \ln \frac{r_{pq}}{r_{p\bar{q}}} \frac{\partial \psi_j(t, \boldsymbol{q})}{\partial n_q}\right) \mathrm{d}s_q \\ &= \int_0^t \mathrm{d}\tau \int_{S_\mathrm{B}} \left(\tilde{G} \frac{\partial \psi_j(\tau, \boldsymbol{q})}{\partial n_q} - \psi_j(\tau, \boldsymbol{q}) \frac{\partial \tilde{G}}{\partial n_q}\right) \mathrm{d}s_q - \int_0^t \mathrm{d}\tau \int_{S_\mathrm{P}} \Pi_j(\tau, \eta) \frac{\partial \tilde{G}}{\partial \tau} \mathrm{d}s_q. \end{aligned} \tag{16}$$

The BIE (16) is based on the source-sink distribution approach. It can be changed to one based on the source distribution approach by extending the fluid domain into the interior of the wetted surface:

$$2\pi\psi_j(t, \boldsymbol{p}) + \int_{S_\mathrm{B}} \sigma_j(t, \boldsymbol{q}) \ln \frac{r_{pq}}{r_{p\bar{q}}} \mathrm{d}s_q = \int_0^t \mathrm{d}\tau \int_{S_\mathrm{B}} \sigma_j(\tau, \boldsymbol{q}) \tilde{G} \mathrm{d}s_q - \int_0^t \mathrm{d}\tau \int_{S_\mathrm{P}} \Pi_j(\tau, \eta) \frac{\partial \tilde{G}}{\partial \tau} \mathrm{d}s_q \tag{17}$$

where σ_j is the source density.

Taking the derivative of Eq.(17) with respect to normal vector $\boldsymbol{n}_p$ on the point $\boldsymbol{p}$, one gets the source density equation

$$-\pi\sigma_j(t, \boldsymbol{p}) + \int_{S_\mathrm{B}} \sigma_j(t, \boldsymbol{q}) \frac{\partial}{\partial n_p} \ln \frac{r_{pq}}{r_{p\bar{q}}} \mathrm{d}s_q = \int_0^t \mathrm{d}\tau \int_{S_\mathrm{B}} \sigma_j(\tau, \boldsymbol{q}) \frac{\partial \tilde{G}}{\partial n_p} \mathrm{d}s_q - \int_0^t \mathrm{d}\tau \int_{S_\mathrm{P}} \Pi_j(\tau, \eta) \frac{\partial^2 \tilde{G}}{\partial z \partial \tau} \mathrm{d}s_q \tag{18}$$

Through Eqs.(17)~(18) the radiation potential ψ_j $(j = 7, \ldots, 6 + N_\mathrm{P})$ can be solved. Substituting ψ_j to the second equation of Eq.(6), one obtains the 3D frequency-domain potential

$$\phi_j(x, y, z) = \psi_j(t(x), y, z) \mathrm{e}^{-\mathrm{i}\omega t(x)} \tag{19}$$

The flowchart for solving the mixed BVP using the 2.5D method is depicted in Fig.1. The BIE (16) or (17) derived from the mixed BVP are completely new. Comparing Eq.(16) with the BIE derived from the Neumann BVP (Ma *et al*., 2005), one can find that there is an additional term related to fluctuating air pressure in the right-hand-most of Eq.(16), while the rest terms in two BIE are the same. One can even observe that the air pressure related term is a free surface memory term rather than an instantaneous one, which suggests that the influence of the fluctuating air pressure on the water or sidehulls is exerted through the radiation wave. On the other hand, comparing Eq.(17) with the BIE derived from the Dirichlet BVP (Guo *et al*., 2017), one can discover that the sidehulls have both instantaneous (the second term on the left-hand side of Eq.(17)) and free surface memory (the first term on the right-hand side of Eq.(17)) effects. Obviously, the sidehulls should have impacts

on the solution of the air cushion pressure.

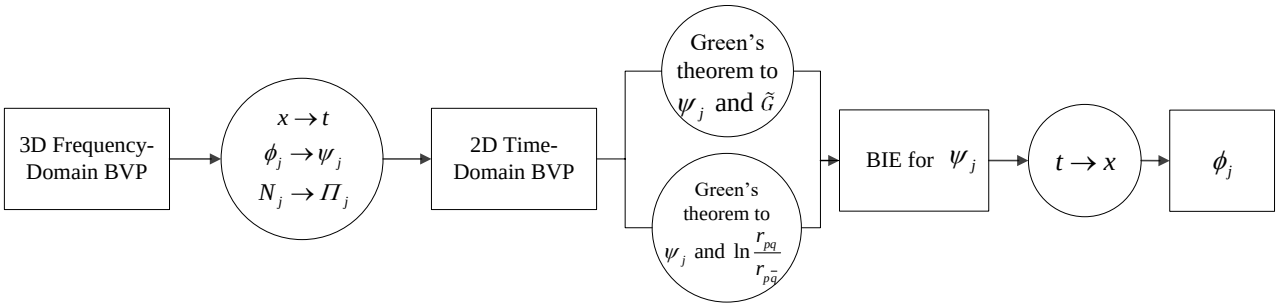

Figure 1. The flowchart for solving the mixed BVP using the 2.5D method.

2.3. The computational complexity and numerical stability of the 2.5D method

As compared with the 3D methods, the major advantage of the 2.5D method is its higher computational efficiency. The analysis and comparison of computational complexity of the 2.5D method with the 3D methods can be roughly drawn out as follows.

Let M_s be the number of sidehull or air cushion sections; N_A and N_B be the number of panels on each air cushion and sidehull section, respectively; $f(k)$ and $F(k,\theta)$ be the integrand of the 2.5D method and the 3D Green's function, respectively. Then similar to the computational complexity of the catamaran sidehulls (Duan *et al*., 2000; Guo *et al*., 2015), the computational complexity of the 2.5D method and the 3D methods for the SES can be written as, respectively

$$P_{2.5\mathrm{D}} = O\left(M_s \times (N_\mathrm{A} + N_\mathrm{B})^2 \times T\left(\int_0^\infty f(k)\mathrm{d}k\right)\right) \tag{20}$$

$$P_{3\mathrm{D}} = O\left({M_s}^2 \times (N_\mathrm{A} + N_\mathrm{B})^2 \times T\left(\int_0^\pi \mathrm{d}\theta \int_0^\infty F(k,\theta)\mathrm{d}k\right)\right) \tag{21}$$

where $T(\cdot)$ represents the computational time for calculating the functions in the brackets. As M_s is normally much larger than one, the computational complexity of the 2.5D method is much less than the 3D methods. In numerical practice, generally the 2.5D method only takes a few minutes, while the 3D methods such as the 3D Rankine source method (Zhang et al., 2011) normally requires a few hours for solving the same problem.

It is worth noting that the matrix of the system equations generated by the abovementioned boundary element methods (BEM) is fully populated and unsymmetrical, which can significantly reduce the computational efficiency with the growth of panel number. Actually, the fast Fourier transform (FFT) methods (Zhang *et al*., 2011) or wavelet function methods (Karimi *et al*., 2005b; Karimi, 2006) can be employed to further enhance the efficiency of BEM. The investigation on this topic is beyond the scope of this paper, and will be carried out in our future works.

The numerical stability of the 2.5D method must be concerned due to that the instability might occur when the ship hulls are not wall-sided (Dai and Duan, 2008). The main cause of the numerical instability is considered to be related with the high numerical wave number near the free surface in the free-surface memory term of the 2D time domain Green's function. To enhance the numerical stability of the 2D time domain Green's function, Duan (1995) set the source density near the free-surface to be zero. Dai and Duan (2008) proposed another two approaches to improve the numerical stability. One is to truncate the infinity upper limit of the integral with respect to wave number in the free-surface memory term to a finite value. The other is to use the implicit method

for evaluating the integral of the free-surface memory term with respect to time instead of the explicit method. More recently, Guo *et al*. (2018a; 2018b) incorporated the viscous dissipation effects into the free-surface equation and then developed a novel 2D time domain Green's function, which was proved to have better numerical stability in evaluating the interaction between waves and floating bodies with flare angles. Nonetheless, the SES to be studied in this paper is almost wall-sided and not subjected to the issue of numerical instability, so no special treatments are needed. If the 2.5D method would be used for floating bodies with flare angles, the developments in Guo *et al*. (2018a; 2018b) should be implemented.

3. Motion equations for the SES

To validate the solution of the mixed BVP solved using the 2.5D method, the motion equations for the SES are briefly introduced in this section, through which the motion response and the fluctuating air pressure can be solved after the hydrodynamic parameters are given by the 2.5D method. Without loss of generality, the 5-DOF motions (the surge is always neglected in the 2.5D methods) of a SES advancing in regular waves of arbitrary directions are considered, though only the heave and pitch motion of a SES in head waves will be investigated in the next section.

3.1. Air dynamic equations

It is assumed that the variation of the fluctuating air pressure in the cushion along the vertical direction is not significant in the SES and so the air pressure can be approximated by

$$\hat{p}(x,y) \cong \frac{1}{h}\int_0^h p(x,y,z)\mathrm{d}z \tag{22}$$

where h is the height of the air cushion; $p(x,y,z)$ is the fluctuating air pressure in the cushion that satisfies the Helmholtz equation

$$\nabla^2 p + k_\mathrm{a}^2 p = 0 \tag{23}$$

where $k_\mathrm{a} = \omega/c$, c is the sound speed.

Substituting Eq.(23) into Eq.(22), one obtains

$$\left(\frac{\partial^2}{\partial x^2} + \frac{\partial^2}{\partial y^2} + k_\mathrm{a}^2\right)\hat{p}(x,y) = -\frac{1}{h}\frac{\partial p}{\partial z}\Big|_{z=0}^{z=h} \tag{24}$$

Taking Eq.(2) into account and using the momentum equation, Eq.(24) comes to

$$\sum_{j=7}^{6+N_\mathrm{P}} \eta_j \left(\frac{\partial^2}{\partial x^2} + \frac{\partial^2}{\partial y^2} + k_\mathrm{a}^2\right) n_j(x,y) = -\frac{\mathrm{i}\omega\rho_\mathrm{a}}{\rho_\mathrm{w} g h} w\Big|_{z=0}^{z=h} \tag{25}$$

where ρ_a is the density of air cushion, w the air flow velocity along the vertical direction in the cushion.

Multiplying Eq.(25) by $N_i(x,y)$, $i = 7,\ldots,6+N_\mathrm{P}$, and integrating the resulting equation with respect to x,y on the horizontal section of the air cushion leads to

$$\eta_i\left(k_\mathrm{a}^2 - 4\pi^2\left(\left(\frac{\alpha}{l}\right)^2 + \left(\frac{\beta}{b}\right)^2\right)\right)\iint_{S_\mathrm{P}} n_i^2(x,y)\,\mathrm{d}x\mathrm{d}y = \frac{\omega^2\rho_\mathrm{a}}{\rho_\mathrm{w} g h}\left(\iint_{S_\mathrm{D}} n_i(x,y)(\eta_3 - x\eta_5 + y\eta_4)\,\mathrm{d}x\mathrm{d}y - \right.$$

$$\left.\iint_{S_\mathrm{P}} n_i(x,y)\zeta(x,y)\,\mathrm{d}x\mathrm{d}y + \sum_{j=1}^{N_\mathrm{out}} n_i(x_j,y_j) q_j^\mathrm{out} - \sum_{j=1}^{N_\mathrm{in}} n_i(x_j,y_j) q_j^\mathrm{in}\right) \tag{26}$$

where N_out and N_in are the number of air leakage holes and/or gaps and the number of air charge inflow holes, respectively; q_j^out and q_j^in are the air leakage and inflow rate through j-th hole (gap), respectively; (x_j,y_j) the centroid of j-th hole (gap), $\zeta(x,y)$ is the unsteady waves on the interface, which can be decomposed into

$$\begin{cases}\zeta(x,y)=\zeta_{\mathrm{I}}(x,y)+\zeta_{\mathrm{D}}(x,y)+\zeta_{\mathrm{R}}(x,y)+\zeta_{\mathrm{P}}(x,y)=\zeta_{\mathrm{I}}(x,y)+\sum_{j=0}^{6+N_{\mathrm{P}}}\eta_j\zeta_j(x,y)\\ \zeta_{\mathrm{I}}(x,y)=\eta_0\mathrm{e}^{-\mathrm{i}k_0(x\cos\theta+y\sin\theta)}\\ \zeta_{\mathrm{D}}(x,y)=\eta_0\zeta_0(x,y)=-\frac{\eta_0}{\mathrm{g}}\left(\mathrm{i}\omega-U\frac{\partial}{\partial x}\right)\phi_0(x,y,0)\\ \zeta_{\mathrm{R}}(x,y)=\sum_{j=2}^{6}\eta_j\zeta_j(x,y)=-\frac{1}{\mathrm{g}}\sum_{j=2}^{6}\eta_j\left(\mathrm{i}\omega-U\frac{\partial}{\partial x}\right)\phi_j(x,y,0)\\ \zeta_{\mathrm{P}}(x,y)=\sum_{j=7}^{6+N_{\mathrm{P}}}\eta_j\zeta_j(x,y)=\sum_{j=7}^{6+N_{\mathrm{P}}}\eta_j\left(n_j(x,y)-\frac{1}{\mathrm{g}}\left(\mathrm{i}\omega-U\frac{\partial}{\partial x}\right)\phi_j(x,y,0)\right)\end{cases}\tag{27}$$

where θ is the incident wave angle, and k_0 the wave number. The first term on the right hand side of Eq.(27) is the incident wave, while the rest terms are the disturbed waves due to unsteady motions and the fluctuating air pressure of the SES.

There are N_{P} air dynamic equations in Eq.(26), in which only motion or pressure amplitudes $\eta_j, j=2,\ldots,6+N_{\mathrm{P}}$ remain unknown. Eq.(26) actually builds up connections between motion responses and the fluctuating air pressure.

3.2. Motion equations for the SES

The 5-DOF motion equations for the SES can be formulated as

$$\sum_{j=2}^{6+N_{\mathrm{P}}}\left(-\omega^2\left(M_{ij}+A_{ij}\right)+\mathrm{i}\omega B_{ij}+C_{ij}\right)\eta_j=F_i,\quad i=2,\ldots,6\tag{28}$$

where M_{ij}, A_{ij}, B_{ij}, C_{ij} are the mass or inertial moment of the SES, added mass, damping, restoring force matrix, respectively, and $M_{ij}=0, C_{ij}=0$ for $j>6$; F_i the wave fore along the i-th direction. As done in well-known linear potential formulation, A_{ij} and B_{ij} are obtained through following equations

$$\begin{cases}A_{ij}=\mathrm{Re}\{\Lambda_{ij}\}/\omega^2\\ B_{ij}=-\mathrm{Im}\{\Lambda_{ij}\}/\omega\end{cases}\tag{29}$$

$$\Lambda_{ij}=-\mathrm{i}\omega\rho_{\mathrm{w}}\iint_{S_{\mathrm{B}}}\phi_j n_i\mathrm{d}s+\rho_{\mathrm{w}}U\iint_{S_{\mathrm{B}}}\phi_j m_i\mathrm{d}s-\rho_{\mathrm{w}}U\int_{C_A}\phi_j n_i\mathrm{d}l\tag{30}$$

where C_A is the stern section of the SES. The wave force F_i could be decomposed into

$$F_i=F_i^{\mathrm{I}}+F_i^{\mathrm{D}}+F_i^{\mathrm{P}}\tag{31}$$

where $F_i^{\mathrm{I}}, F_i^{\mathrm{D}}$ and F_i^{P} are the F-K force, diffraction force and air dynamic force on the wet deck, respectively. Their expressions are given as following

$$\begin{cases}F_i^{\mathrm{I}}=-\eta_0\cdot\mathrm{i}\rho_{\mathrm{w}}\omega_0\iint_{S_{\mathrm{B}}}\phi_0 n_i\mathrm{d}s\\ F_i^{\mathrm{D}}=\eta_0\cdot\Lambda_{i0}\\ F_i^{\mathrm{P}}=-\rho_{\mathrm{w}}\mathrm{g}\sum_{j=7}^{6+N_{\mathrm{P}}}\eta_j\iint_{S_{\mathrm{D}}}n_j(x,y)n_i(x,y)\,\mathrm{d}x\mathrm{d}y\end{cases}\tag{32}$$

Eq.(26) and Eq.(28) together with Eqs. (29)- (32) make up the closed equations for the SES, through which one can solve all motions and pressure amplitudes $\eta_j, j=2,\ldots,6+N_{\mathrm{P}}$.

4. Application of the 2.5D method for solving the BVPs of the PACSCAT

In this section the solution of the mixed BVP obtained using the 2.5D method is validated through two cases, which evaluates the radiation wave on the interface due to fluctuating air pressure and solves heave and pitch response as well as air dynamics of a PACSCAT running in regular head waves. Since the PACSCAT runs in head waves, the variation of the fluctuating air pressure along the transverse direction can be ignored. So two

orthogonal Fourier modes from Eq.(3): $N_7(x,y)=1$ and $N_8(x,y)=\sin(\pi x/l)$ ($x_m \cong 0$ for the PACSCAT) are used in the following studies. Table 1 shows the principal parameters of the PACSCAT model. More detailed information and the body plan for the PACSCAT can be found in Guo *et al*. (2015).

Table 1. Principal parameters of the PACSCAT model (Guo *et al*., 2015).

Parameters	Value	Parameters	Value
Mass (M)	145 kg	Moment of inertia for pitch (M_{55})	77.4 kg·m^2
Overall length (L)	3.0 m	Static cushion overpressure (p_0)	760 Pa $(F_{rl}=0.73)$
Beam (B)	0.7 m		510 Pa $(F_{rl}=1.0)$
Cushion length (l)	2.5 m	Air inflow rate (Q_0)	150 m^3/h
Cushion breadth (b)	0.24 m	Fan characteristic value $(\partial Q_{in}/\partial p)$	-7.2E-5 $m^3/(s\cdot Pa)$

4.1. Radiation wave on the interface due to fluctuating air pressure

As shown in Eqs.(26)~(27), the radiation wave ζ_P on the interface due to fluctuating air pressure on the interface of the SES could have an impact on the motion responses, which suggests the importance of accurately predicting it. In many publications, however, the radiation wave ζ_P was neglected (Faltinsen, 2005), or approximated by solving the Dirichlet BVP (Doctors, 1976; Xie *et al*., 2008; Guo *et al*., 2017). Here we would like to compare the radiation wave ζ_P of the PACSCAT by solving the Dirichlet BVP with the one by solving the mixed BVP. Both of the mixed BVP and the Dirichlet BVP are solved using the 2.5D method.

Fig.2 depicts the radiation wave profiles at the central longitudinal section $y=0$ for the cases of $F_{rl}=1.0$ and $\omega\sqrt{l/g}=3.38$. In the figure, (*a*) and (*b*) show the real and imaginary part of ζ_7 while (*c*) and (*d*) give the real and imaginary part of ζ_8. In addition, the label 'Dirichlet BVP' and 'Mixed BVP' indicate that the radiation waves are obtained by solving the Dirichlet and mixed BVP, respectively.

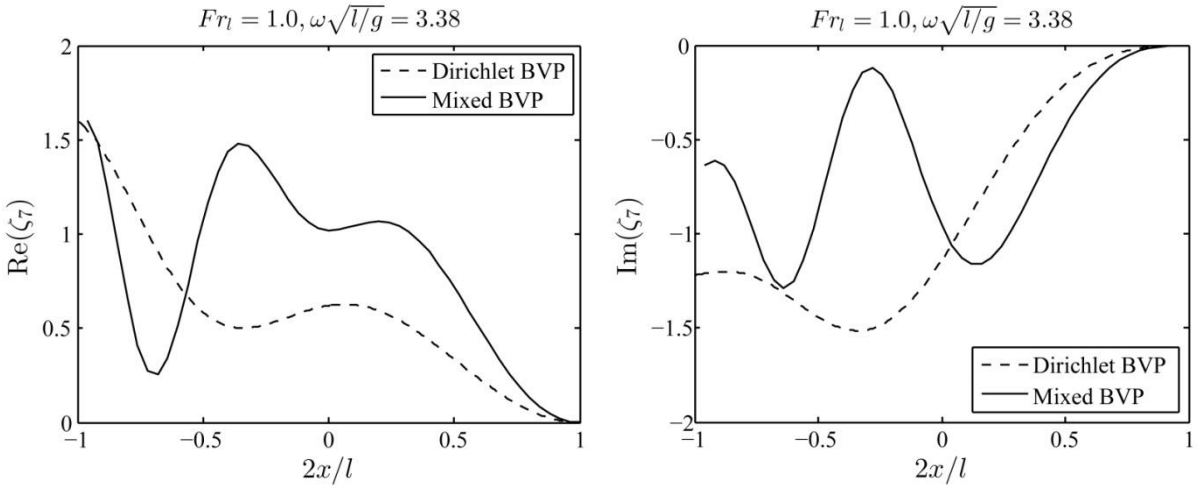

(*a*) (*b*)

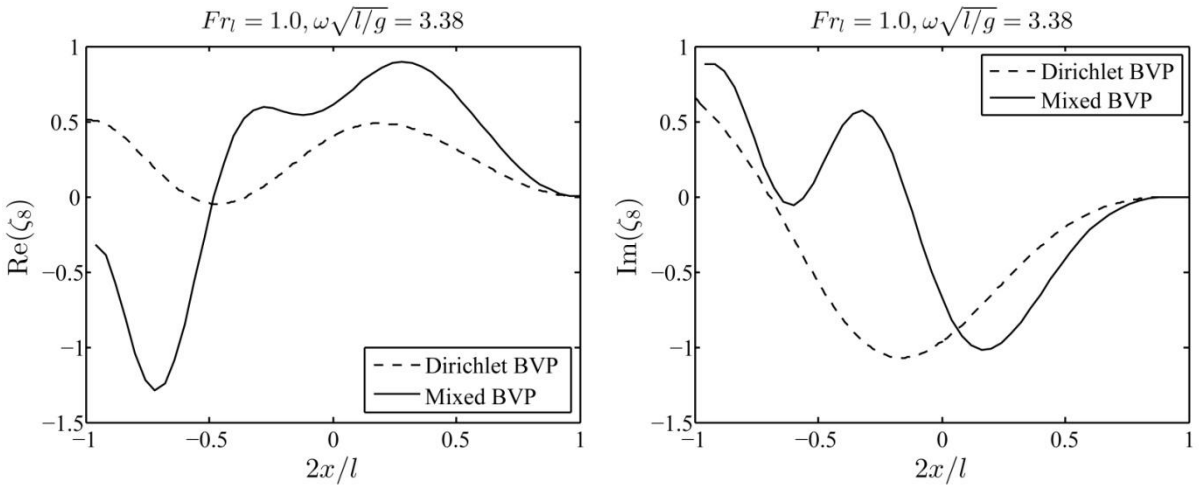

(*c*) (*d*)

Figure 2. The profiles of radiation waves ζ_7 and ζ_8 (defined in Eq.(27)) due to fluctuating air pressure at $y = 0$ for $F_{rl} = 1.0$ and $\omega\sqrt{l/g} = 3.38$. 'Dirichlet BVP' and 'Mixed BVP' indicate the radiation waves obtained by solving the Dirichlet and mixed BVP, respectively. (*a*) Real part of ζ_7; (*b*) Imaginary part of ζ_7; (*c*) Real part of ζ_8; (*d*) Imaginary part of ζ_8.

From Fig.2, one can find that the radiation wave from solving the Dirichlet BVP is very different from solving the mixed BVP, or more specifically, the latter is steeper than the former. This means that the coupling between the fluctuating air pressure and sidehulls has significant influence on the radiation wave on the interface, and the selective omission of the coupling effects could bring inevitable errors to the hydrodynamics of the air cushion. The numerical results in this case also confirm the importance and necessity on solving the complete mixed BVP to accurately predict the hydrodynamics of a SES.

4.2. Motion responses of the PACSCAT

The significant influence of coupling between the fluctuating air pressure and sidehulls on the radiation wave profiles on the interface was demonstrated in Fig.2. It might be more interesting to investigate how the coupling effects make the difference in the seakeeping performance and air dynamics of the PACSCAT.

Fig.3 compares numerical results on the heave, pitch and fluctuating air pressure responses of the PACSCAT with the experimental data marked as 'EFD' under Froude number $F_{rl} = 0.73$ and 1.0. The results labeled by '$\zeta = \zeta_\mathrm{I} + \zeta_\mathrm{P}(\mathrm{D})$' are obtained from the potential model that considers the incident wave and the radiation wave due to fluctuating air pressure on the interface by solving the Dirichlet BVP, while the sidehull involved waves are not taken into account. The results labeled by '$\zeta = \zeta_\mathrm{I} + \zeta_\mathrm{D} + \zeta_\mathrm{R} + \zeta_\mathrm{P}(\mathrm{M})$' are obtained from the potential model that considers all possible waves on the interface, including the incident wave, diffraction and radiation wave of sidehulls, the radiation wave due to fluctuating air pressure by solving the mixed BVP. The former is a simplified model that was utilized in Doctors (1976) and Xie et al. (2008), while the latter is a completely new model formed from the motion equations proposed in this work. The results labeled by 'CFD' were obtained from the RANS (Reynolds-averaged Navier-Stokes equations) solver given by

Yang *et al.* (2015), in which the bow fingers and stern seal bags of the PACSCAT are modeled as rigid bodies. Note that only the heave and pitch motion of the PACSCAT were presented in Yang *et al.* (2015), while the fluctuating air pressure was not given.

From Fig.3 (*a*)~(*b*) one can observe that two potential models generate the almost same heave RAOs in large encountered frequencies ($\omega\sqrt{l/g} > 4$), but the results from model '$\zeta = \zeta_{\mathrm{I}} + \zeta_{\mathrm{D}} + \zeta_{\mathrm{R}} + \zeta_{\mathrm{P}}(\mathrm{M})$' have slightly better agreement with EFD data in the vicinity of natural frequency of the PACSCAT. Almost the same trend is obtained for the pitch RAO as shown in Fig.3 (*c*)~(*d*). The RANS solver underestimate the heave RAO under low encountered frequencies but overestimate it under high encountered frequencies. On the other hand, the RANS solver desirably predicts the pitch RAO under low encountered frequencies but significantly overestimates it under high encountered frequencies. From Fig.3 (*e*)~(*f*), it is more evident that the model '$\zeta = \zeta_{\mathrm{I}} + \zeta_{\mathrm{D}} + \zeta_{\mathrm{R}} + \zeta_{\mathrm{P}}(\mathrm{M})$' significantly improves the numerical results of the fluctuating air pressure in the vicinity of the resonance frequency. In contrast, the model '$\zeta = \zeta_{\mathrm{I}} + \zeta_{\mathrm{P}}(\mathrm{D})$' overestimates the resonance peak of the fluctuating air pressure at $F_{rl} = 0.73$, while underestimates that at $F_{rl} = 1.0$.

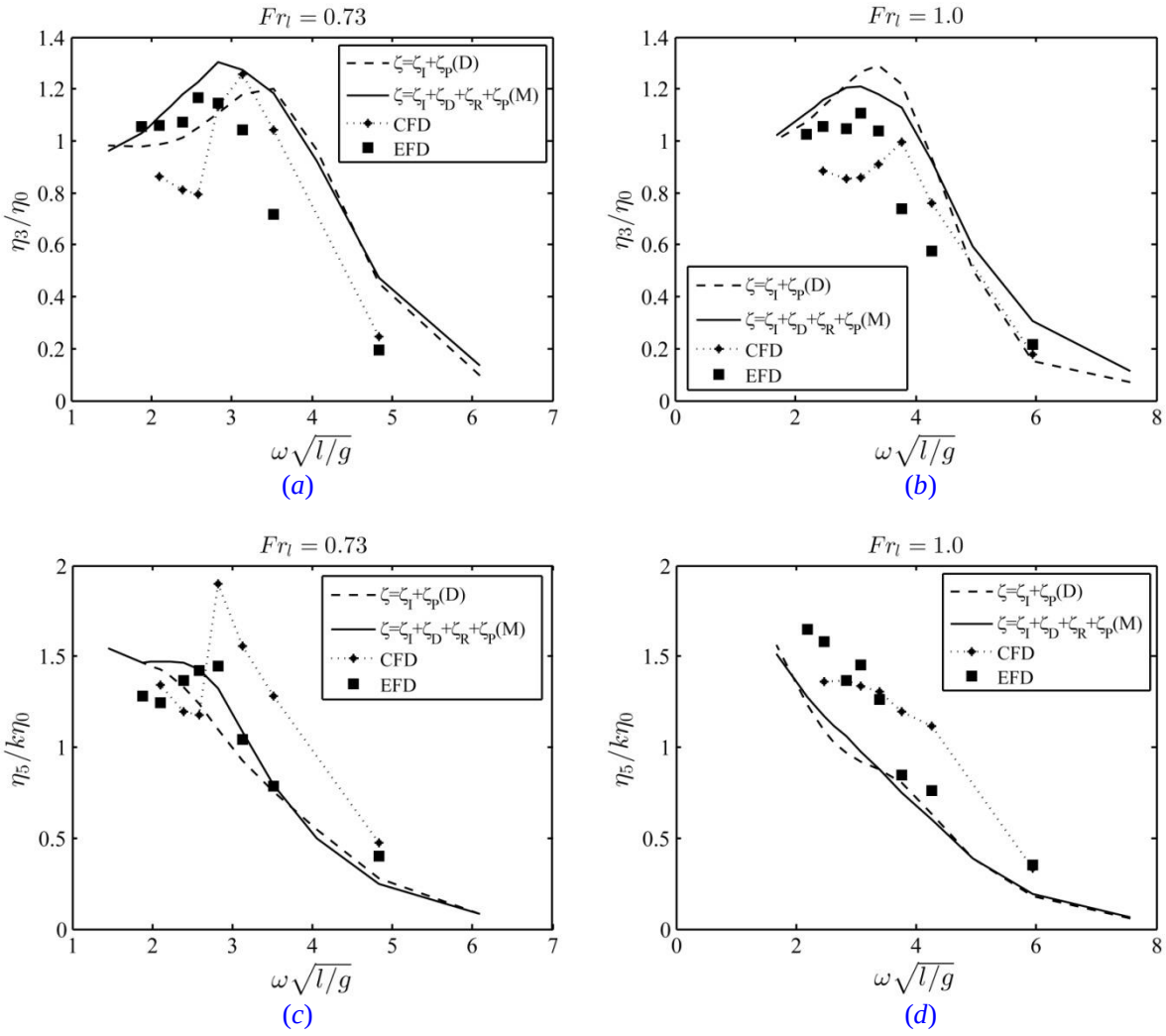

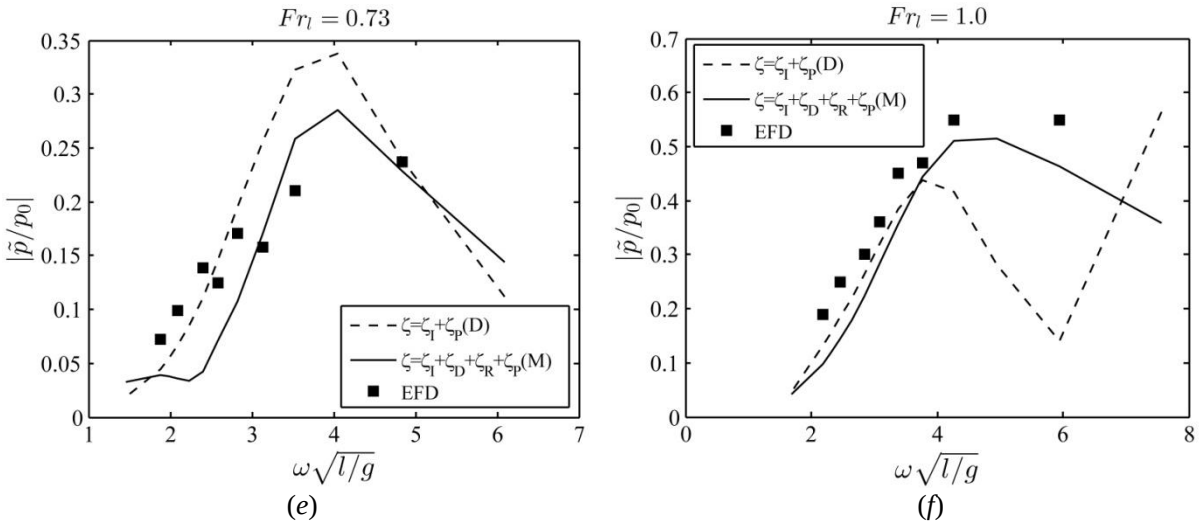

Figure 3. A comparison of numerical results with experimental data marked as 'EFD' on seakeeping performance of the PACSCAT under Froude number $F_{rl} = 0.73$ and 1.0. '$\zeta = \zeta_I + \zeta_P(D)$' represents the numerical results obtained from the model that considers the incident wave and the radiation wave due to fluctuating air pressure on the interface by solving the Dirichlet BVP, while the sidehull induced waves are not taken into account. '$\zeta = \zeta_I + \zeta_D + \zeta_R + \zeta_P(M)$' are obtained from the model that considers all possible waves on the interface, including the incident wave, diffraction and radiation wave of sidehulls, the radiation wave due to fluctuating air pressure by solving the mixed BVP. 'CFD' are the CFD results from Yang *et al.* (2015). (*a*~*b*) Heave RAO; (*c*~*d*) Pitch RAO; (*e*~*f*) Fluctuating air pressure RAO.

The numerical results suggest that the coupling effects could have significant influence on the air cushion dynamics, and the 2.5D method is helpful to capture the effects as well as to improve the numerical results on motion response and the fluctuating air pressure.

5. Conclusions

This paper firstly presents the 2.5D method to solve the mixed BVP of a SES consisting of homogeneous Neumann boundary condition on the sidehulls and nonhomogeneous Dirichlet boundary condition on the interface. This kind of problem has never been dealt with by the 2.5D method before. The newly developed 2.5D method allows one to consider the coupling between the fluctuating air pressure and sidehulls, which is usually ignored in other publications.

The solution of the mixed BVP obtained using the 2.5D method is validated by applying it on a special SES – PACSCAT through two cases. The first case is to evaluate the radiation wave due to fluctuating air pressure on the interface. The numerical results confirm that the radiation wave from solving the Dirichlet BVP (Doctors, 1976; Xie *et al.*, 2008; Guo *et al.*, 2017) is very different from solving the complete mixed BVP, i.e. the sidehull effects have significant impact on the radiation wave and should not be ignored. The second case is employing the 2.5D method to calculate the relative hydrodynamic parameters of the PACSCAT and solve the motion equations to obtain the seakeeping performance of the PACSCAT. The numerical results suggest that the 2.5D method is able to capture the sidehull effects and to improve the predicted results of the fluctuating air pressure.

The effectiveness of the 2.5D method for solving the mixed BVP is primitively validated in this paper, and

more numerical tests are expected to be carried out in the future.

Acknowledgments: This project is supported by the National Natural Science Foundation of China (Grant no.51509053, no.51579056 and no.51739001). The second author wishes to thank the Chang Jiang Visiting Chair professorship of Chinese Ministry of Education, supported and hosted by the HEU.

References

Bhushan, S., Mousaviraad, M., Stern F., 2017. Assessment of URANS surface effect ship models for calm water and head waves. *Applied Ocean Research*, **67**: 248-262.

Connell, S.B., Milewski, M.W., Goldman, B., Kring, C.D., 2011. Single and multi-body surface effect ship simulation for T-Craft design evaluation. Proceedings of the 11th International Conference on Fast Sea Transportation. FAST 2011. Honolulu, Hawaii, USA, pp.130–137.

Dai, Y.S., Duan, W.Y., 2008. Potential Flow Theory of Ship Motions in Waves. 1st ed., The National Defense Industries Press: Beijing, China, pp. 248–249.

Doctors, L.J., 1976. The effect of air compressibility on the nonlinear motion of an air-cushion vehicle over waves. Proceedings of the 11th ONR Symposium on Naval Hydrodynamics. UCL, London, UK, pp.373–388.

Duan, W.Y., 1995. Nonlinear Hydrodynamic Forces Acting on a Ship Undergoing Large Amplitude Motions. Ph.D. Thesis, Harbin Engineering University, Harbin, China.

Faltinsen, O., Zhao, R., 1991. Numerical predictions of ship motions at high forward speed. *Philos. Trans. R. Soc. Lond, A*, **334**: 241-252.

Faltinsen, O.M., 2005. Hydrodynamics of high-speed marine vehicles, 1st ed., Publisher: Cambridge University Press, UK, p.141- 163.

García-Espinosa, J., Capua, D.D., Serván-Camas, B., et al., 2015. A FEM fluid–structure interaction algorithm for analysis of the seal dynamics of a Surface-Effect Ship. *Computer Methods in Applied Mechanics & Engineering*, **295**: 290-304.

Guo, Z.Q., Ma, Q.W., Yang, J.L., 2015. A seakeeping analysis method for a high-speed partial air cushion supported catamaran (PACSCAT). *Ocean Eng*., **110**: 357-376.

Guo, Z.Q., Ma, Q.W., Sun, H.B., Hao, H.B., 2017. 2.5D method for pulsating pressure induced waves on the free surface. Proc. of 27th International Ocean and Polar Engineering Conference (ISOPE 2017), San Francisco, California, USA, June 25-30, p.1029-1033.

Guo, Z.Q., Ma, Q.W., Qin, H.D., 2018a. A time-domain Green's function for interaction between water waves and floating bodies with viscous dissipation effects. *Water*, **10**, 72.

Guo, Z.Q., Ma, Q.W., Yu, S.R., Qin, H.D., 2018b. A body-nonlinear Green's function method with viscous dissipation effects for large-amplitude roll of floating bodies. *Applied Sciences*, **8**(4), 517.

Karimi, H.R., Maralani, P.J., Lohmann, B., et al., 2005a. H∞ control of parameter-dependent state-delayed systems using polynomial parameter-dependent quadratic functions. *International Journal of Control*, **78**(4): 254-263.

Karimi, H.R., Moshiri, B., Lohmann, B., Maralani, P.J., 2005b. Haar wavelet-based approach for optimal control of second-order linear systems in time domain. *Journal of Dynamical & Control Systems*,**11**(2): 237-252.

Karimi, H.R., 2006. Optimal vibration control of vehicle engine-body system using haar functions. *International Journal of Control Automation & Systems*, **4**(6): 714-724.

Karimi, H.R., Duffie, N.A., Dashkovskiy, S., 2010. Local capacity h_{∞} control for production networks of autonomous work systems with time-varying delays. *Automation Science & Engineering IEEE Transactions on*, **7**(4): 849-857.

Lee, C.H., Newman, J.N., 2015. An extended boundary integral equation for structures with oscillatory free-surface pressure. *International Journal of Offshore & Polar Engineering*, **1**: 347-353.

Ma, S., Duan, W.Y., Song, J.Z., 2005. An efficient numerical method for solving '2.5D' ship seakeeping problem. *Ocean Eng*, **32**(8–9): 937–960.

Xie, N., Vassalos, D., Jasionowski, A., Sayer, P., 2008. A seakeeping analysis method for an air-lifted vessel. *Ocean Eng*, **35**: 1512-1520.

Yang, J.L., Sun, H.B., Guo, Z.Q., 2015. Study on motion of partial air cushion support catamaran in regular waves. J. Huazhong Univ. Sci. & Tech. (Natural Science Edition), **43**(11): 104-109.

Zhang, S., Weems, K., Lin, W.M., 2011. Solving nonlinear wave-body interaction problems with the pre-corrected fast fourier transform (pFFT) method. In: Proceedings of the 11th International Conference on Fast Sea Transportation. FAST 2011. Honolulu, Hawaii, USA, pp. 153-160.

Zhang, L., Wang, S., Karimi, H.R., Jasra, A., 2015. Robust finite-time control of switched linear systems and application to a class of servomechanism systems. *IEEE/ASME Transactions on Mechatronics*, **20**(5): 2476-2485.